Syntheses, Reactivity Studies and the Catalytic Properties of a Series of Tetraosmium−Gold Mixed-Metal Clusters

Yat Li[a] and Wing-Tak Wong*[a]

Keywords: Osmium / Gold / Clusters / Electrochemistry / Carbonylations

Treatment of the mixture of $[Os_4(\mu\text{-}H)_4(CO)_{12}]$ and $[AuPPh_3Cl]$ with excess triethylamine afforded three novel tetraosmium–gold mixed-metal clusters, $[Os_4Au_2(\mu\text{-}H)_2(CO)_{11}(PPh_3)_3]$ (**4**), $[Os_4Au_3(\mu\text{-}H)_3(CO)_{11}(PPh_3)_3]$ (**5**), and $[Os_4Au_4(\mu\text{-}H)_2(CO)_{11}(PPh_3)_4]$ (**6**) in moderate yields. Cluster $[Os_4Au(\mu\text{-}H)_3(CO)_{11}(NMe_3)(PPh_3)]$ (**2**) was also obtained in a similar reaction in the presence of trimethylamine *N*-oxide. They were fully characterized by different spectroscopic techniques, and the solid-state structures were established by X-ray analysis. These dimetallic clusters exhibit an osmium/gold ratio ranging from 1 to 4. Their electronic absorption properties, electrochemistry, and catalytic properties, as a result of the oxidative carbonylation of aniline, were investigated in terms of the Os/Au ratio.

Introduction

The chemistry of transition mixed-metal clusters containing (phosphane)gold units has been well established in the past decade.[1−14] The initial interest in these clusters stemmed from the perceived isolobal analogy between a hydride and a (phosphane)gold group.[15] This interest has continued to develop since they were found to be potential homogeneous dimetallic catalysts. The introduction of heterometallic metal−metal bonding into these clusters leads to an increase in the polarity of the molecule, which probably results in the enhancement of the catalytic activity. Examples of catalysis by mixed-metal clusters that contain (phosphane)gold groupings have been reported.[16−24] Previously, we reported that $[Os_4Au(\mu\text{-}H)_3(CO)_{12}(PPh_3)]$ (**1**) catalyzes the oxidative carbonylation of aniline to give methyl phenylcarbamate in methanol with good conversion and selectivity.[25] This paper reports in detail the syntheses and characterization of a series of novel tetraosmium−gold mixed-metal clusters with Os/Au ratios ranging from 1 to 4. A better understanding of the role of gold atoms in the dimetallic system has been developed through the study of their electronic absorption properties, electrochemistry, and catalytic properties.

[a] Department of Chemistry, The University of Hong Kong, Pokfulam Road, Hong Kong, P. R. China
Fax: (internat.) + 852/25472933
E-mail: wtwong@hkucc.hku.hk

Results and Discussion

The preparation of **1**−**6** is summarized in Scheme 1. In fact, the synthesis and characterization of **1** and **3** were reported by Lewis in the 1980s,[26] and it is surprising that the high-nuclearity tetraosmium−gold mixed-metal clusters can also be isolated in a similar reaction with an excess amount of triethylamine. It appears that the protons in $[Os_4(\mu\text{-}H)_4(CO)_{12}]$ were successively eliminated by Et_3N as $[Et_3NH]^+$, the vacant sites formed were then simultaneously filled up by $[AuPPh_3]^+$ to afford a series of osmium−gold mixed-metal clusters. The formation of gold clusters is also favorable in a reducing environment; as a result, the Au−Au bonds are formed in **3**−**6**. Nevertheless, further elimination of protons in **3**−**6** is improbable due to the limited reducing power of Et_3N. Recently, Raithby et al. have reported on the deprotonation of the cluster $[Os_4H(CO)_{12}(AuPR_3)_3]$ in the presence of $[AuPR_3]^+$ in an attempt to produce tetragold clusters, but met with little success. They alternatively used the chelated gold salt $[Au_2(Ph_2PCH_2PPh_2)Cl_2]$ to treat with the anion $[Os_4H_4(CO)_{11}]^{2-}$ and give $[Os_4(\mu\text{-}H)_2(CO)_{11}\{Au_2(dppm)\}_2]$.[27] The successful isolation of **5** and **6** proves that the deprotonation of (hydrido)osmium clusters in the presence of $[Au(PPh_3)]^+$ could be an efficient method for preparing the high-nuclearity osmium−gold mixed-metal clusters in a systematic manner.

These osmium−gold mixed-metal clusters were isolated with relatively small yields, even in the presence of excess $[AuPPh_3Cl]$, where the equilibrium between formation and decomposition of these mixed-metal clusters was established. Changing in stoichiometry of $[AuPPh_3Cl]$ has no significant effect on the product yields. This deprotonation reaction is also thought to be successive. Independent depro-

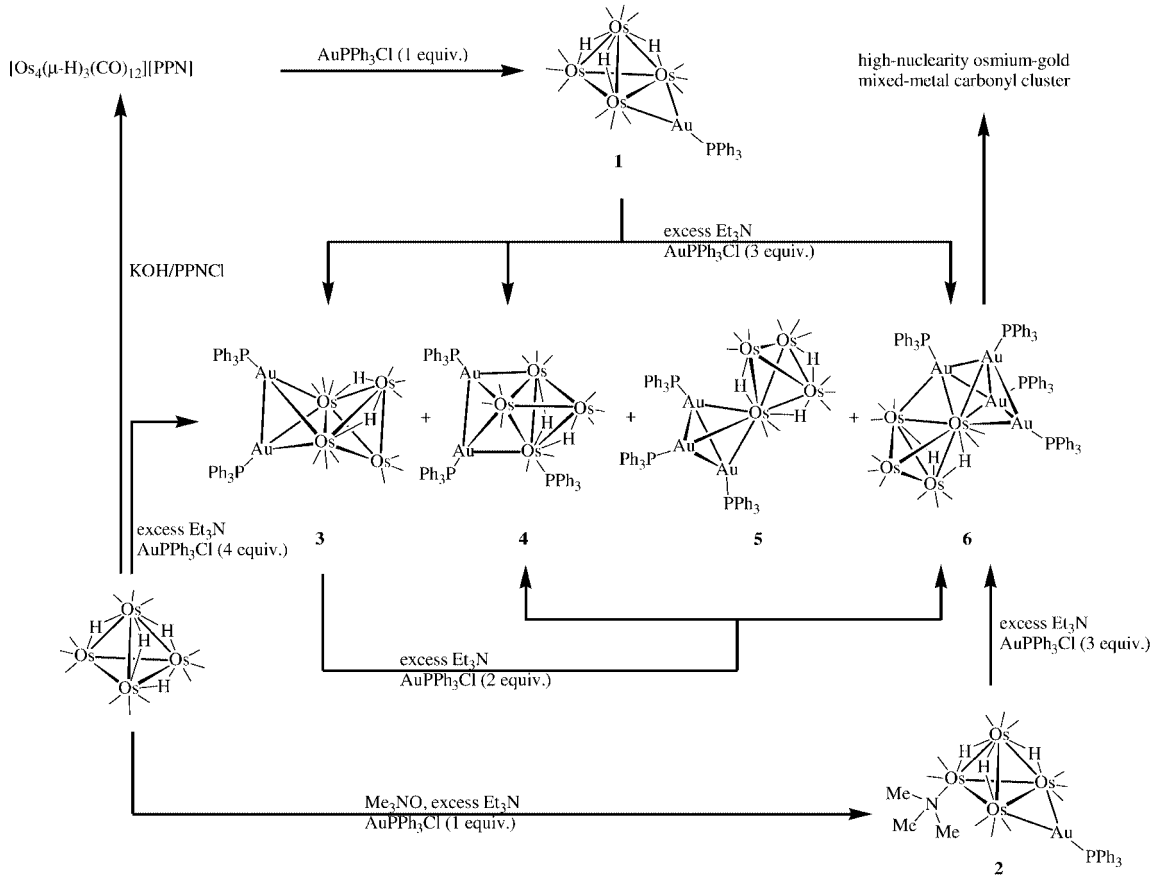

Scheme 1

tonation of all isolated compounds with an excess of the [$AuPPh_3Cl$] compound were studied (Scheme 1). This showed that **1**−**3** can be further converted into **4** or **6** in moderate yields. In addition, the deprotonation of **6** with an excess of [$AuPPh_3Cl$] gives an insoluble microcrystalline solid, which is believed to be a high-nuclearity osmium−gold mixed-metal carbonyl cluster with an Os/Au ratio of 3:2. The nature of this compound is still under active investigation.

Structural Characterization

The molecular structure of **2** is depicted in Figure 1. Four osmium atoms define a distorted tetrahedron. The Os(1)−Os(2) bond is symmetrically bridged by Au(1), with a bite angle Os(1)−Au(1)−Os(2) of 64.47(4)° and Os−Au bond lengths of 2.768(2) and 2.753(2) Å. The dihedral angle between the planes of Os(1)−Os(2)−Os(3) and Os(1)−Au(1)−Os(2) is 120.2° which is slightly larger than the corresponding value 109.5° that is observed in **1**.[25] The trimethylamine is terminally bonded to Os(3) with an Os(3)−N(1) distance of 2.24(2) Å which is similar to the value of 2.25(1) Å in $[Os_4(\mu\text{-}H)_4(CO)_{10}(NMe_3)\{\eta^1\text{-}NC_5H_4(N{=}N)C_6H_5\}]$.[28] The Os−Os bond lengths are observed in the range of 2.803(2)−3.009(2) Å, where the hydrido- or ligand-bridged Os−Os bonds are significantly elongated. The hydride ions bridging the Os(1)−Os(3) and Os(2)−Os(3) edges are chemically equivalent, which corresponds to the double integral hydride signal that is observed in the ^1H NMR spectrum of **2**.

The molecular structure of **4** is depicted in Figure 2, where the tetraosmium tetrahedron is terminally coordinated with eleven carbonyl ligands. Two {$AuPPh_3$} ligands bridge two adjacent Os−Os edges to form a distorted square pyramid [Au(1), Au(2), Os(1), Os(2), and Os(4)] which shares the plane Os(1)−Os(2)−Os(4) with the tetraosmium tetrahedron. A similar metal framework was observed in $[Os_4(CO)_{13}(AuPEt_3)_2]$.[29] The Au(1)−Au(2) bond [3.055(1) Å] is slightly shorter than the corresponding one in $[Os_4(CO)_{13}(AuPEt_3)_2]$ [3.128(1) Å], but is significantly longer than that in **3** [2.793(4) Å] where the two $AuPR_3$ groups bridge the same Os−Os edge.[26] An extra triphenylphosphane ligand is terminally bonded to Os(4), having an Os(4)−P(1) bond length of 2.362(6) Å. The gold− and osmium−triphenylphosphane protons give two multiplets with an integral ratio of 2:1 in the ^1H NMR spectrum of **4**. However, the P atoms of three different chemical environments in **4** give only one ^{31}P NMR signal. This is probably due to the fluxional behavior of the {$AuPPh_3$} ligand at room temperature on the NMR timescale which is frequently found in homo- and heteronuclear clusters.[30−32] Low-temperature ^{31}P NMR spectroscopy was carried out for **4** at 223 K and the signal resolved into two singlets with an intensity ratio of 2:1 (Figure 3). The formation of

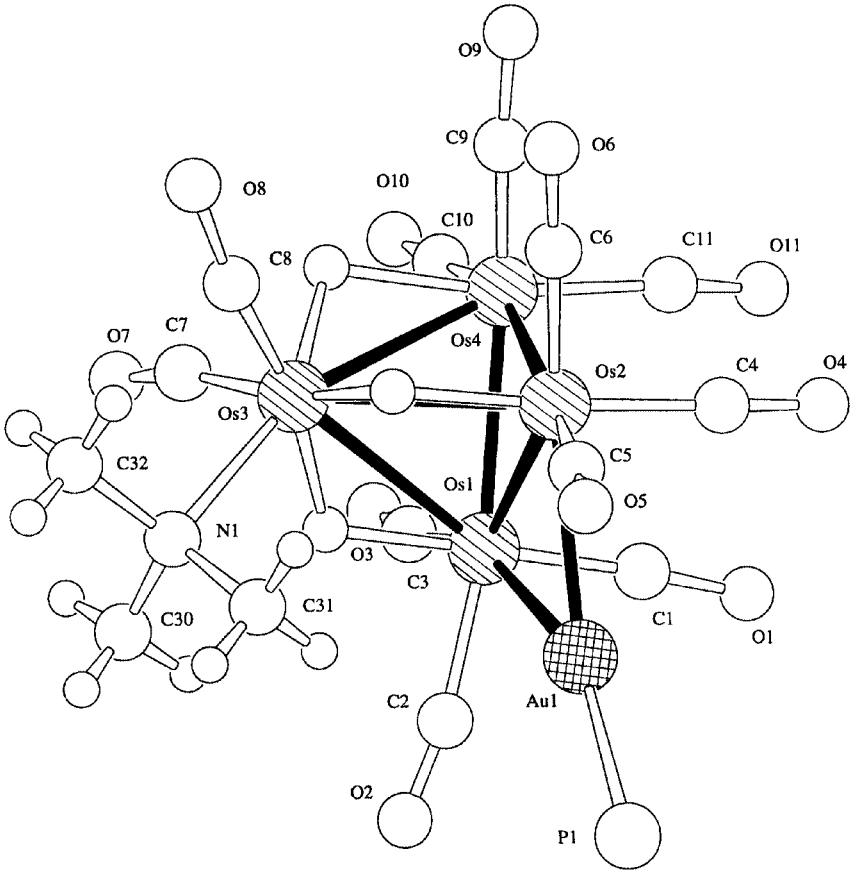

Figure 1. Simplified molecular structure of $[Os_4Au(\mu\text{-}H)_3(CO)_{11}(NMe_3)(PPh_3)]$ (**2**) with the atom numbering scheme (phenyl groups are omitted for clarity)

osmium−triphenylphosphane may be due to a triphenylphosphane impurity in the starting material, a similar observation has been reported in the case of $[Os_3(CO)_8(PPh_3)\{Au(PPh_3)\}(2\text{-}NHC_5H_4N)]$.[33] However, the moderate yield of **4** implies that the Au−P bond cleavage probably occurs in the reaction, giving free triphenylphosphane ligands.

The ^1H NMR spectrum of **5** shows that one double doublet and two triplet peaks with an integral ratio of 2:1:2, which corresponds to the 45 phenyl protons, are observed in the aromatic region. The protons are differentiated into *ortho*-, *meta*-, and *para*-phenyl protons according to their coupling patterns and integral values. A broad signal is found in the hydride region; therefore, variable-temperature ^1H NMR spectroscopic studies were carried out for **5**. At 223 K, the broad signal was resolved into three sharp singlet peaks with equal integral values. The ^{31}P NMR spectrum of **5** exhibits a singlet peak attributable to the three equivalent $\{AuPPh_3\}$ ligands.

To the best of our knowledge, cluster **5** is the first example of a cluster with an Os_4Au_3 metal core. The X-ray analysis shows that the gold atoms are terminally coordinated to one of the vertices of the tetraosmium tetrahedron and bonded with each other by Au−Au bonds to form another tetrahedron [Au(1), Au(2), Au(3), and Os(1)] (Figure 4). The Au−Au bond lengths lie in the range of 2.796(3)−2.860(2) Å, which is significantly shorter than the values that were observed in **4**. The two tetrahedrons are fused together by sharing the central Os(1) atom, which has the highest metal−metal connectivity, with three Os−Os contacts and three Os−Au contacts. This kind of coordination mode is rare and significantly different from the metal core arrangement observed in $[Ru_4Au_3(\mu_3\text{-}H)(CO)_{12}(PPh_3)_3]$.[34] The dihedral angle between the planes Os(1)−Os(2)−Os(4) and Os(1)−Au(1)−Au(2) is 79.3°, while the angle of Au(3)−Os(1)−Os(3) is 148.0°. It seems that the tetrahedrons bend towards each other. In terms of electron counting, each Au atom is simply considered as a one-electron donor, and the tangential gold−gold interactions are ignored. Overall, the molecule of **5** has 60 cluster valence electrons, and is isoelectronic with $[Os_4(\mu\text{-}H)_4(CO)_{12}]$ in the neutral oxidation state. It is surprising that **5** was not observed in the deprotonation reactions of **1**−**4**. It is reasonable to believe that the presence of the

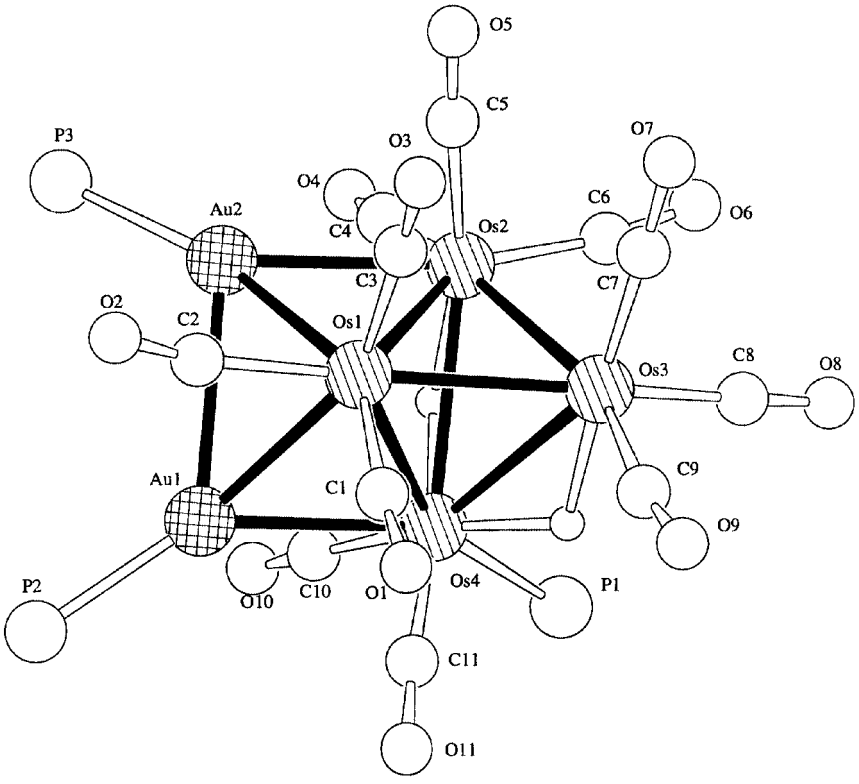

Figure 2. Simplified molecular structure of $[Os_4Au_2(\mu\text{-}H)_2(CO)_{11}(PPh_3)_3]$ (**4**) with the atom numbering scheme (phenyl groups are omitted for clarity)

bridging $\{AuPPh_3\}$ ligand in **1**−**4** probably makes the reaction unfavorable; an extra amount of energy is required to break the Os−Au bonds before the formation of **5**.

Cluster **6** exhibits aromatic ^1H NMR signals that are similar to those of **5**. Variable-temperature ^1H NMR studies were conducted for **6** at 223 K, the broad hydride peak was resolved into two sets of two sharp singlets, which correspond to the isomers of **6** in solution, named **6a** and **6b**, due to the disposition of hydrides. Three possible isomers of **6** are shown in Figure 5. It suggests that the ^1H NMR signal of the hydrido bridge on the Os*−Os bond is slightly different from the bridge on the Os−Os bond, where Os* is more electron-rich. The hydride ions of **6a** are most likely arranged in type C which gives relatively separated ^1H NMR signals at $\delta = -18.97$ and -14.52 ppm. Since the hydride signals of **6b** are relatively downfield and have a similar chemical shift, it is probably attributed to a type A isomer. Similarly, the fluxional behavior of $\{AuPPh_3\}$ ligands was also identified in the ^{31}P NMR spectrum of **6** at room temperature. The broad signal was resolved into eight singlet signals of equal intensity in the low-temperature ^{31}P NMR spectrum at 233 K, which is consistent with the existence of **6a** and **6b**.

The molecular structure of **6** is depicted in Figure 6. Similarly, the metal framework consists of a tetraosmium tetrahedron, and the Au(3) atom asymmetrically bridges the Os(1)−Os(2) edge. The other three gold atoms are terminally bonded to Os(1), and bonded with each other by Au−Au bonds to give a trigonal bipyramid that is defined by the atoms [Os(1), Au(1), Au(2), Au(3), and Au(4)]. The Au−Au bond lengths are observed in the range of 2.804(2)−3.069(2) Å, and are similar to the equivalent values observed in $[Os_4(\mu\text{-}H)_2(CO)_{11}\{Au_2(dppm)\}_2]$. As a result, the metal framework may be viewed as a tetrahedron fused with a trigonal bipyramid by sharing the Os(1) atom and connected by the Os(1)−Au(3) bond. The novel metal core geometry of **6** is significantly different from the arrangement observed in $[Os_4(\mu\text{-}H)_2(CO)_{11}Au_2(dppm)_2]$. The Os(1) atom has the highest metal−metal connectivity, with three Os−Os contacts and four Os−Au contacts. An overall of 60 cluster valence electrons is also observed in **6**.

Electrochemistry

The electrochemistry of **1**−**6** and the starting materials $[Os_4(\mu\text{-}H)_4(CO)_{12}]$ and $[N(PPh_3)_2][Os_4(\mu\text{-}H)_3(CO)_{12}]$ were investigated in acetonitrile using cyclic voltammetry and controlled potential coulometry with tetrabutylammonium hexafluorophosphate (TBAHFP) as the supporting electrolyte. The results of the voltammetric and controlled potential coulometry experiments are summarized in Table 1.

The cyclic voltammogram of **1** contains two irreversible anodic waves with a large potential difference between the

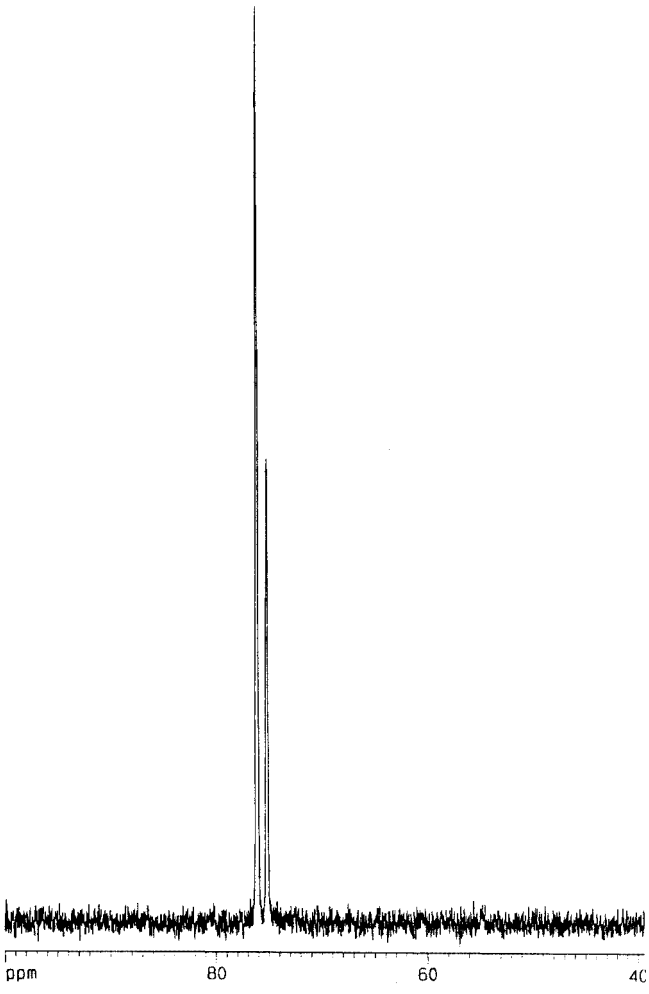

Figure 3. Low-temperature (223 K) ^{31}P NMR spectrum of $[Os_4Au_2(\mu\text{-}H)_2(CO)_{11}(PPh_3)_3]$ (**4**)

first and second oxidation peaks (around 1 V) (Figure 7, a) Reduction of **1** is believed to be difficult, as no cathodic wave is located within the solvent limit. The electrochemical behavior of **1** and $[PPN][Os_4(\mu\text{-}H)_3(CO)_{12}]$ is similar. The incorporation of the $\{AuPPh_3\}$ ligand seems to have no significant effect on the energy level of the HOMO of $[PPN][Os_4(\mu\text{-}H)_3(CO)_{12}]$.

The isolobal parent cluster $[Os_4(\mu\text{-}H)_4(CO)_{12}]$ unexpectedly has a different redox behavior to **1**. The cyclic voltammogram of $[Os_4(\mu\text{-}H)_4(CO)_{12}]$ contains an irreversible cathodic wave and an irreversible anodic wave. Accurate data of the controlled potential coulometry cannot be obtained because of the limited solubility of $[Os_4(\mu\text{-}H)_4(CO)_{12}]$ in organic solvents. Compared to **1** and $[PPN][Os_4(\mu\text{-}H)_3(CO)_{12}]$, the reduction of $[Os_4(\mu\text{-}H)_4(CO)_{12}]$ is believed to be more feasible but the oxidation is more difficult. The large positive shift (600 mV) in the oxidation potential implies that the substitution of the isolobal $\{AuPPh_3\}$ for hydrogen in $[Os_4(\mu\text{-}H)_4(CO)_{12}]$ seems to be able to activate the tetraosmium cluster towards the oxidation reaction by raising the HOMO.

Although the metal frameworks of **1** and **2** are exactly the same, the substitution of the carbonyl ligand by a trimethylamine ligand leads to different electrochemical behavior. The cyclic voltammogram of **1** exhibits both irreversible cathodic and anodic peaks (Figure 7, b). There is a positive shift in both the cathodic and anodic peaks with reference to those with equivalent values of **1**. This suggests that the coordination of the trimethylamine ligand lowers both the HOMO and the LUMO, which makes the oxidation more difficult while the reduction becomes easier.

The redox properties of the known compound **3** were also studied as a reference. The electrochemical behavior of **3** is similar to that of **1**. There are two irreversible anodic peaks, but no cathodic peak was located within the solvent limit. Controlled potential coulometry revealed that each oxidation peak involves 1 F/mol of **3**, which is different from the double-electron oxidation process observed in **1**. The first oxidation potential of **3** is similar to the value of **1**; however, it displays a 520 mV positive shift in the second oxidation potential. This shows that the monoanion of **3** undergoes a second oxidation, which is much easier since the oxidation process involves only one electron. The difference in the redox properties of **3** from **1** might be attributed to the presence of the Au−Au bond, which might alter the relative positions of the HOMO and LUMO.

As expected, the redox behavior of **4** is significantly different from that of **3**. This is probably due to the different arrangement in the metal core and the ligand effect of an extra osmium−triphenylphosphane ligand, which is similar to the case of the trimethylamine ligand observed in **2**. In fact, the cyclic voltammogram of **4** closely resembles that of **2**. The less negative reduction potential of **4** suggests that the osmium−triphenylphosphane ligand significantly lowers the LUMO of the cluster and makes the reduction easier. However, the oxidation potential of **4** is similar to the value obtained in **3** and **1**. The HOMO and LUMO of these kinds of mixed-metal clusters are believed to be metal- and ligand-based, respectively.

The cyclic voltammograms of **5** and **6** are similar, and also similar to that of **3**. Both exhibit two irreversible anodic waves. Comparing the oxidation potentials of $[Os_4(\mu\text{-}H)_4(CO)_{12}]$, **1**, **3**, **5**, and **6** (Os/Au range from 0 to 4), they display a slightly negative shift in the first oxidation potential as the number of gold atoms increase. This is probably because the delocalization of electrons in the high-nuclearity cluster is more significant, and the effect of losing an electron can be shared by more metal centers, making the oxidation easier. The energy level of the metal-based HOMO is believed to be raised, corresponding to the decrease in the oxidation potential. The second oxidation potential of **6** is similar to the equivalent value of **3**. However, **5** exhibits a significantly lowered second oxidation potential, with a negative shift of ca. 300 mV as compared with **6**. This suggests that the novel metal core arrangement of **5** might interrupt the arrangement of the HOMO and LUMO, making the cluster more reactive towards oxidation. It is difficult to correlate the reduction potential with the change in gold atom numbers, since the cathodic

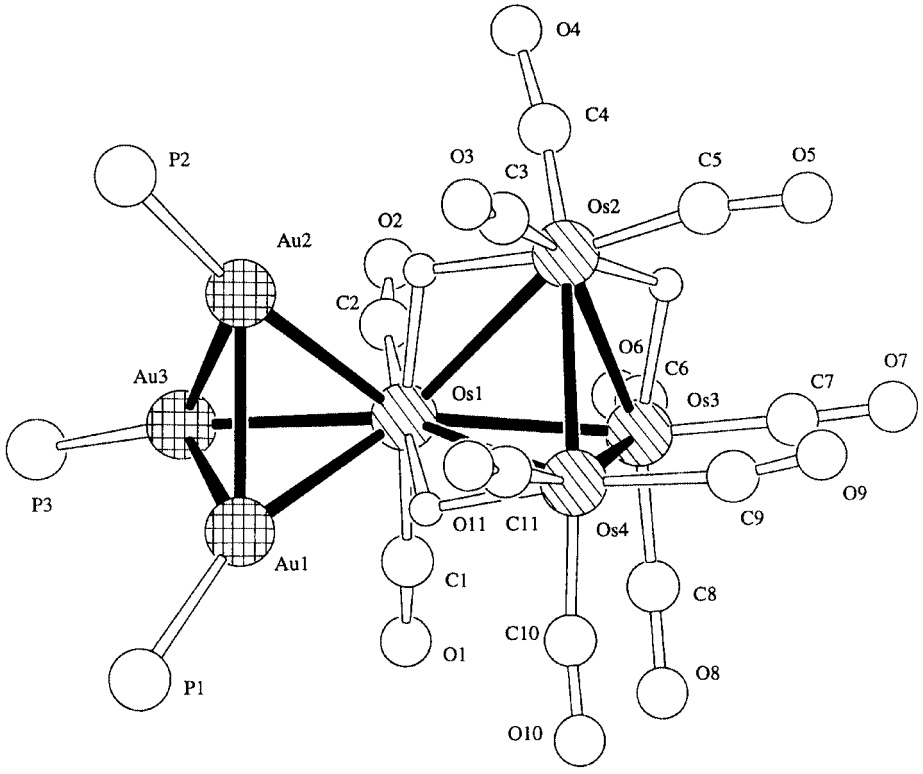

Figure 4. Simplified molecular structure of $[Os_4Au_3(\mu\text{-}H)_3(CO)_{11}(PPh_3)_3]$ (**5**) with the atom numbering scheme (phenyl groups are omitted for clarity)

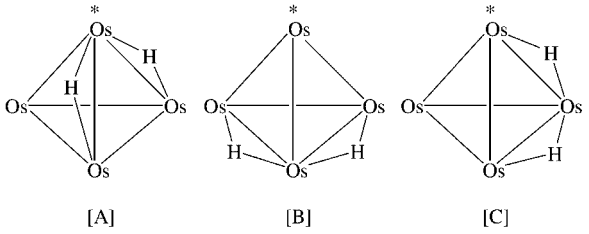

Figure 5. Three possible isomers of **6** (*: Os extensively connected with tetragold cluster)

wave of **1**, **3**, and **5** are not observed within the solvent limit.

Electronic Absorption Properties

Clusters **1**−**6** displayed a trend of color changes from yellow to red in the solid state, prompting us to examine them by optical spectroscopy. Table 2 presents the electronic absorption spectroscopic data for **1**−**6** together with the cluster $[PPN][Os_4(\mu\text{-}H)_3(CO)_{12}]$ in dichloromethane at ambient temperature.

The energy absorption bands of these osmium−gold mixed-metal clusters are within the range of 320 to 401 nm. Cluster **2** exhibits the highest energy absorption band at 320 nm. This implies that the energy gap between the HOMO and LUMO is the largest and is consistent with the large peak-to-peak separation (ca. 2.5 V) of the redox potentials observed in its cyclic voltammogram. On the other hand, both of the clusters **4** and **6** have the lowest energy absorption band at 401 nm, which corresponds to the small HOMO−LUMO energy gap. Consequently, the peak-to-peak separation of the redox waves (ca. 1.9 V) observed in their cyclic voltammograms is significantly small in comparison to the value of **2**. The similar separations in **4** (1.91 V) and **6** (1.96 V) suggest that the energy gap between HOMO and LUMO might be directly proportional to the separation of redox potentials in the cyclic voltammogram, in cases where the HOMO−LUMO involved in the electronic transition is assumed to have the same orbitals where the redox reaction occurs. According to this assumption, it might be possible to estimate the redox potential out of the solvent limit by using the electronic absorption spectroscopic data as a reference. As the electronic energy absorption bands of **1**, **3**, and **5** are observed in the range of 320 to 401 nm, the separation of their first anodic peak and first cathodic peak is believed to be within the range of 1.9 to 2.5 V. The transition energy gap between the HOMO−LUMO seems to decrease slightly as the HOMO is raised due to the increasing number of gold atoms in the cluster (Figure 8). This is fully consistent with their electrochemical behavior. Cluster **5** is an exceptional case, having a high-energy electronic absorption band that is attributable to the large separation of HOMO and LUMO. The reason might be related to the novel coordination mode of the gold atoms.

Catalytic Properties of 1 and 6 towards the Oxidative Carbonylation of Aniline

The catalytic performance of **1** and **6** towards the oxidative carbonylation of aniline in methanol was investigated

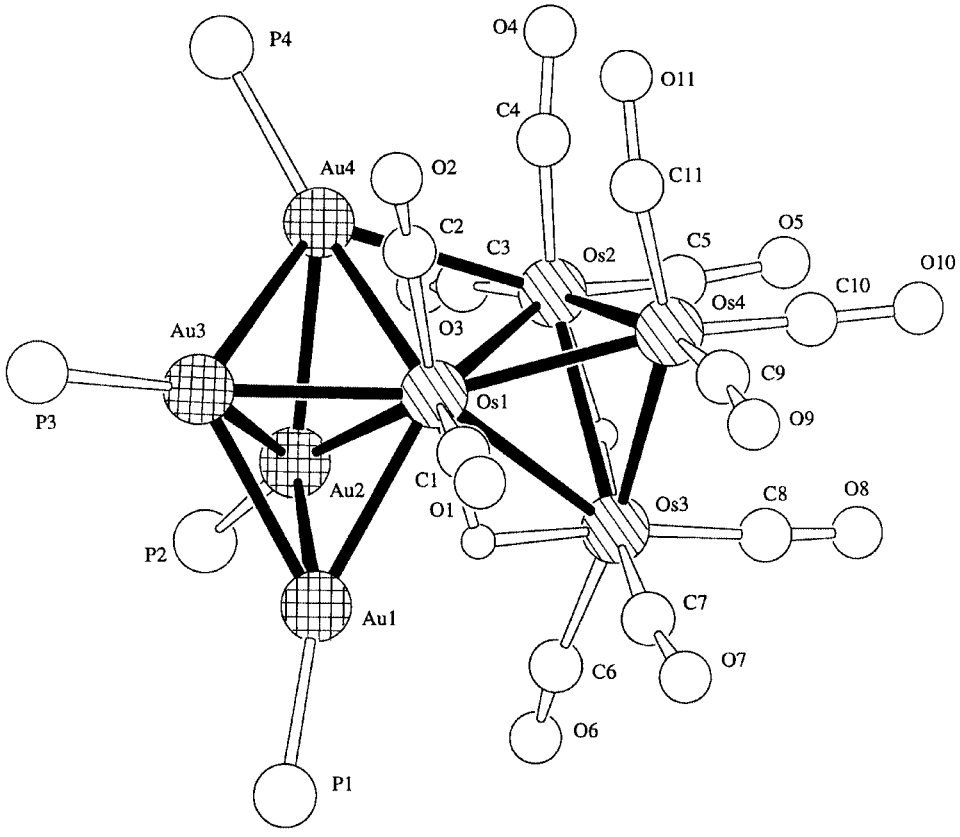

Figure 6. Simplified molecular structure of $[Os_4Au_4(\mu\text{-}H)_2(CO)_{11}(PPh_3)_4]$ (**6**) with the atom numbering scheme (phenyl groups are omitted for clarity)

Table 1. Electrochemical data of **1**−**6** and some starting materials

Cluster[a]	Oxidation		Reduction
	E_{pa2} [V][b]	E_{pa1} [V][b]	E_{pc1} [V][b]
$[Os_4(\mu\text{-}H)_4(CO)_{12}]$[c]	−	0.71	−1.99
$[PPN][Os_4(\mu\text{-}H)_3(CO)_{12}]$	1.01(2)	0.13(2)	−
1	1.11(2)	0.12(2)	−
2	−	0.51(2)	−2.00(2)
3	0.59(1)	0.18(1)	−
4	−	0.13(2)	−1.78(2)
5	0.37(1)	0.14(1)	−
6	0.56(1)	−0.08(1)	−2.02(2)

[a] About 10^{-3} M cluster in 0.1 M TBAHFP in acetonitrile at 298 K, the working electrode was a glassy carbon electrode, the auxiliary electrode and the reference electrode were a platinum wire and $Ag/AgNO_3$ (0 V) under the same conditions, calibrated with ferrocene. Scan rate was 100 $mV \cdot s^{-1}$. [b] E_{pa} and E_{pc} are the anodic and cathodic potentials, respectively, Values in parentheses are Faraday per mol of cluster. [c] Limited solubility in acetonitrile.

[Equation (1)]. The effect of reaction time, temperature, concentration of methanol, pressure (P_{CO} and P_{O_2}) and promoters (sulfuric acid and triphenylphosphane) were studied and optimized. Some selected catalytic results are presented in Table 3. The catalytic properties of the polynuclear and mononuclear homometallic starting materials, including $[Au(PPh_3)Cl]$, $[Os(CO)_3(DEAAB)Cl]$, $[Os(CO)_2(PAN)Cl]$, and $[N(PPh_3)_2][Os_4(\mu\text{-}H)_3(CO)_{12}]$ were also studied under the same conditions as a reference.

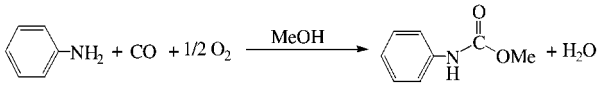

(1)

The catalysts **1** and **6** are active towards the oxidative carbonylation of aniline even without the promoters (Entries 2 and 3). However, the selectivity to carbamate is relatively low. The presence of promoters (triphenylphosphane and sulfuric acid) seems extremely important in achieving a reasonable selectivity in carbamate (Entries 5 and 6). Although catalysts **1** and **6** display slightly different interactions with the promoters, the overall catalytic performance towards the oxidative carbonylation of aniline in yielding carbamate is similar. This suggests that the effect of the osmium/gold ratio on this catalytic reaction is not significant. Consequently, a similar catalytic performance is believed to be found in the catalytic systems involving **2**−**5.**

The catalytic properties of catalysts $[Au(PPh_3)Cl]$ and $[PPN][Os_4(\mu\text{-}H)_3(CO)_{12}]$ are similar (Entries 4 and 7), but much less selective than the dimetallic systems. The synergism of dimetallic catalyst systems is believed to be significant in enhancing the selectivity towards carbamate. Two mononuclear osmium systems $[Os(CO)_2Cl(PAN)]$ and $[Os(CO)_3Cl(DEAAB)]$ were also studied, and exhibited a much lower TOF as compared with the cluster systems. In ad-

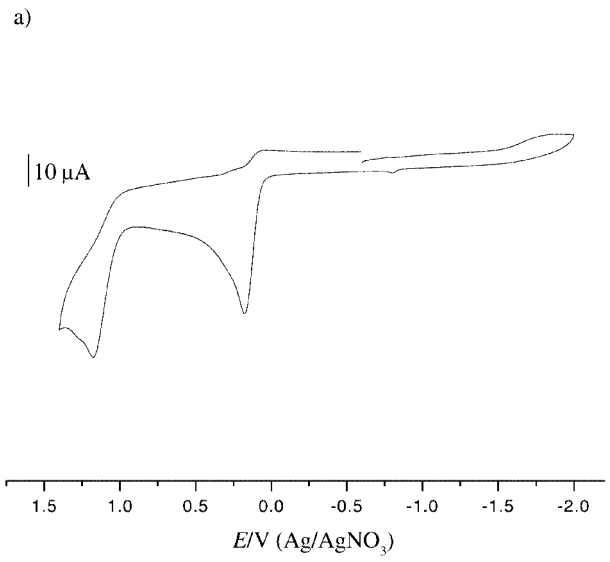

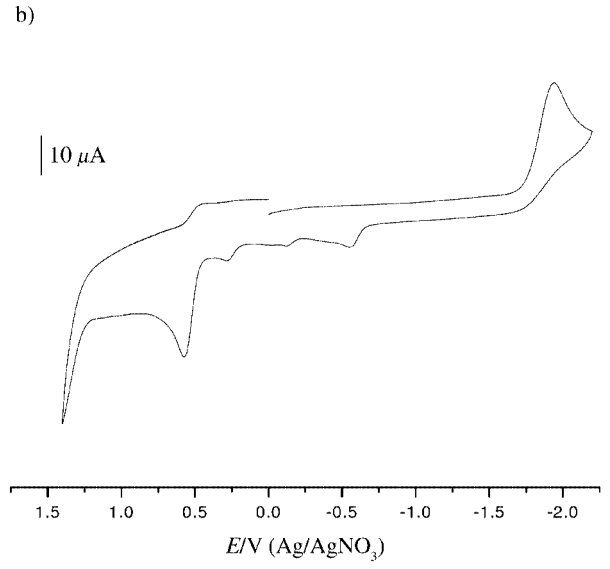

Figure 7. Cyclic voltammogram of a) **1** and b) **2** in acetonitrile, with 0.1 M TBAHFP as the supporting electrolyte, using a glassy carbon working electrode at 298 K; the voltammogram is recorded against an $Ag/AgNO_3$ reference electrode

Table 2. The electronic absorption spectroscopic data for **1**−**6** together with the cluster $[PPN][Os_4(\mu\text{-}H)_3(CO)_{12}]$

Cluster	λ_{max} [nm] (ε [dm^3 mol^{-1} cm^{-1}])[a]	Color
$[PPN][Os_4(\mu\text{-}H)_3(CO)_{12}]$	327 (11000)	yellow
1	330 (14000)	yellow
2	320 (12000)	yellow
3	366 (10000)	red
4	401 (12000)	red
5	334 (8000)[b]	yellow
6	401(11000)[b]	red

[a] In dichloromethane. [b] Shoulder.

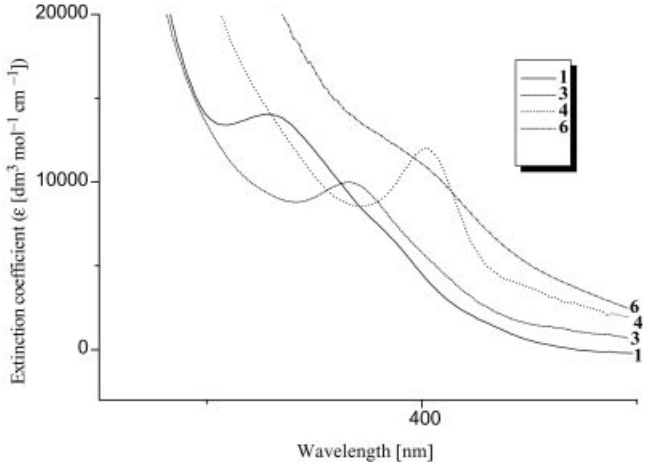

Figure 8. Electronic absorption bands of **1**, **3**, **4**, and **6**

dition, it is interesting to note that the distribution of by-products observed in polynuclear and mononuclear systems is different. Formaniline is the major by-product of mononuclear osmium systems, while the cluster systems favor the formation of azobenzene. This implies that the two systems might follow different catalytic pathways, which supports the proposition that the cluster is the active catalytic species in solution.

Conclusion

A series of novel osmium−gold mixed-metal clusters, exhibiting an osmium/gold ratio range from 1 to 4, were prepared in a systematic manner. The electrochemical studies show that the incorporation of an $\{AuPPh_3\}$ unit may activate the tetraosmium−carbonyl cluster toward oxidation by lowering the oxidation potential. A slightly negative shift of oxidation potential was observed as the number of gold atoms increased. This was further confirmed by the electronic absorption studies. The correlation between the redox behavior and the electronic absorption properties was established. Clusters **1** and **6** catalyze oxidative carbonylation of aniline yielding carbamate with a good activity and selectivity in the presence of promoters. The dimetallic synergism is proved, and the effect of the Os/Au ratio on catalytic performance does not seem to be significant. The dimetallic cluster is believed to be the active catalyst in the solution.

Experimental Section

General Remarks: All reactions and manipulations were carried out under argon using standard Schlenk techniques, except for the chromatographic separations. Solvents were purified by standard procedures and distilled prior to use.[35] Reactions were monitored by analytical thin-layer chromatography (Merck Kieselgel 60 F_{254}), and the products were separated by thin-layer chromatography on plates coated with silica (Merck Kieselgel 60 F_{254}). All chemicals, unless otherwise stated, were purchased commercially and used as

Table 3. Catalytic results of **1**, **6**, and the starting materials towards the oxidative carbonylation of aniline

Entry	Catalyst[a]	Conversion(%)	Selectivity (%)					TOF[b]
			Methyl phenylcarbamate	*N*-Methyl-aniline	Quinazoline	Formaniline	Azobenzene	
1	[PPN][$Os_4(\mu\text{-}H)_3(CO)_{12}$]	35	0	22	0	0	78	210
2	**1**	97	8	0	4	4	46	582
3	**6**	97	9	4	8	4	18	582
4[c]	[PPN][$Os_4(\mu\text{-}H)_3(CO)_{12}$]	99	8	0	5	3	46	594
5[c]	**1**	63	65	10	15	0	0	378
6[c]	**6**	92	41	5	8	0	23	552
7[c]	[$Au(PPh_3)Cl$]	97	13	0	5	1	32	582
8[d]	[$Os(CO)_2Cl$(PAN)]	24	15	16	5	16	8	48
9[d]	[$Os(CO)_3Cl$(DEAAB)]	25	21	10	2	14	6	50

[a] Catalytic conditions: 155 °C, 4 MPa of CO, 2 MPa of O_2, 2 h, 20 mL of methanol. [b] Mol of aniline converted per mol of cluster per hour, catalyst/substrate ≈ 1200. [c] Promoters present (PPh_3/catalyst ≈ 10 and catalyst/H_2SO_4 ≈ 10). [d] PAN: 1-(2-pyridylazo)-2-naphthol; DEAAB: 4-(diethylamino)azobenzene; catalyst/substrate ≈ 600.

received. [$Os_4(\mu\text{-}H)_4(CO)_{12}$] and [$N(PPh_3)_2$][$Os_4(\mu\text{-}H)_3(CO)_{12}$] were prepared by the literature methods.[36−38] Infrared spectra were recorded with a Bio-Rad FTS-135 IR spectrometer, using 0.5 mm calcium fluoride solution cells, ^1H and ^{31}P NMR spectra with a Bruker DPX400 spectrometer using CD_2Cl_2, and referenced to $SiMe_4$ and 85% H_3PO_4, respectively. Variable-temperature ^1H and ^{31}P NMR spectra were obtained with a Bruker DPX500 spectrometer. Positive ionization fast atom bombardment (FAB) mass spectra were recorded with a Finnigan MAT 95 mass spectrometer, using *m*-nitrobenzyl alcohol as the matrix solvent. Electronic absorption spectra were obtained with a Hewlett−Packard 8453 diode array UV/Vis spectrophotometer using quartz cells, with a 1-cm path length at room temperature. Butterworth Laboratories, UK performed the microanalyses. The Energy Dispersive X-ray Analysis measurements were performed with a Scanning Electron Microscope (Leica Cambridge Stereo 360, 20KV).

Synthesis of [$Os_4Au(\mu\text{-}H)_3(CO)_{11}(NMe_3)(PPh_3)$] (2): Solid samples of [$Os_4(\mu\text{-}H)_4(CO)_{12}$] (110 mg, 0.1 mmol) and 1 equiv. of [$AuPPh_3Cl$] (49 mg, 0.1 mmol) were dissolved in 30 mL of dichloromethane; 1 equiv. of Me_3NO was then added dropwise to the solution mixture, followed by several drops of Et_3N at ambient temperature. The solution became yellow after stirring for 15 min, and the solvent was removed under reduced pressure. The residue was chromatographed by TLC using a mixture of *n*-hexane/dichloromethane (1:1, v/v) as eluent. The yellow band of [$Os_4Au(\mu\text{-}H)_3(CO)_{11}(NMe_3)(PPh_3)$] (**2**) was isolated. Yield: ca. 24 mg (15%). ^1H NMR (400 MHz, CD_2Cl_2, 298 K): δ = −25.32 (s, 2 H, hydride), −18.98 (s, 1 H, hydride), 2.95 (s, 9 H, methyl), 7.42 (m, 15 H, phenyl) ppm. ^{31}P NMR (400 MHz, CD_2Cl_2, 298 K): δ = 85.09 (s, PPh_3) ppm. IR [ν(CO)/cm^{-1}; CH_2Cl_2]: $\tilde{\nu}$ = 1933 m, 1975 w, 1983 w, 1989 w, 2024 s, 2028 s, 2039 s, 2074 m. FAB-MS [M^+]: *m*/*z* = 1590. $C_{32}H_{27}AuNO_{11}Os_4P$ (1590.31): calcd. C 24.17, H 1.71, N 0.88; found C 24.3, H 1.7, N 0.9.

Reaction of [$Os_4(\mu\text{-}H)_4(CO)_{12}$] with [$AuPPh_3Cl$] in Excess Et_3N: A solid sample of [$Os_4(\mu\text{-}H)_4(CO)_{12}$] (110 mg, 0.1 mmol) and excess [$AuPPh_3Cl$] (196 mg, 0.4 mmol) were dissolved in 30 mL of dichloromethane under argon. Excess Et_3N was added dropwise to this pale yellow solution, giving a dark brownish red clear solution after stirring for an additional 3 h. The decomposition of products was observed and then the solvent was reduced in vacuo. The residue was filtered, some unchanged [$Os_4(\mu\text{-}H)_4(CO)_{12}$] (32 mg, 0.029 mmol) was recovered. The filtrate was then subjected to preparative TLC using a solution mixture of *n*-hexane/dichloromethane (2:3, v/v) as eluent. The four consecutive orange bands were characterized as [$Os_4Au_2(\mu\text{-}H)_2(CO)_{12}(PPh_3)_2$] (**3**) (10 mg, 5%), [$Os_4Au_2(\mu\text{-}H)_2(CO)_{11}(PPh_3)_3$] (**4**) (9 mg, 4%), [$Os_4Au_3(\mu\text{-}H)_3(CO)_{11}(PPh_3)_3$] (**5**) (7 mg, 3%), and [$Os_4Au_4(\mu\text{-}H)_2(CO)_{11}(PPh_3)_4$] (**6**) (20 mg, 7%). **4**: ^1H NMR (400 MHz, CD_2Cl_2, 298 K): δ = −19.69 (s, 1 H, hydride), −19.66 (s, 1 H, hydride), 7.21 (m, 15 H, $OsPPh_3$), 7.38 (m, 30 H, $AuPPh_3$) ppm. ^{31}P NMR (400 MHz, CD_2Cl_2) 298 K: δ = 76.09 (s, PPh_3); 223 K: 76.10 (s, PPh_3), 75.17 (s, PPh_3) ppm. IR [ν(CO)/cm^{-1}; CH_2Cl_2]: $\tilde{\nu}$ = 1997 m, 2018 s, 2060 m. FAB-MS [M^+]: *m*/*z* = 2251. $C_{65}H_{47}Au_2O_{11}Os_4P_3$ (2251.90): calcd. C 34.67, H 2.10; found C 34.8, H 2.2. **5**: ^1H NMR (400 MHz, CD_2Cl_2) 298 K: δ = −16.52 (br., 3 H, hydride), 6.98 (t, $J_{H,H}$ = 7.35, 18 H, *meta*-PPh_3), 7.22 (t, $J_{H,H}$ = 7.50, 9 H, *para*-PPh_3), 7.30 (dd, $J_{H,H}$ = 7.90, 18 H, *ortho*-PPh_3); 223 K: δ = −17.87 (s, 1 H, hydride), −16.68 (s, 1 H, hydride), −14.13 (s, 1 H, hydride) ppm. ^{31}P NMR (400 MHz, CD_2Cl_2, 298 K): δ = 56.97 (s, PPh_3) ppm. IR [ν(CO)/cm^{-1}; CH_2Cl_2]: $\tilde{\nu}$ = 1985 m, 2003 s, 2032 s, 2062 s. FAB-MS [M^+]: *m*/*z* = 2449. $C_{65}H_{48}Au_3O_{11}Os_4P_3$ (2449.71): calcd. C 31.87, H 1.97; found C 31.9, H 1.9. **6**: ^1H NMR (400 MHz, CD_2Cl_2): 298 K: δ = −16.46 (br., 2 H, hydride), 6.98 (t, $J_{H,H}$ = 7, 24 H, *meta*-PPh_3), 7.22 (t, $J_{H,H}$ = 7, 12 H, *para*-PPh_3), 7.32 (dd, $J_{H,H}$ = 13, 24 H, *ortho*-PPh_3); 223 K: **6a**: δ = −18.97 (s, 1 H, hydride), −14.52 (s, 1 H, hydride); **6b**: δ = −18.59 (s, 1 H, hydride), −18.24 (s, 1 H, hydride) ppm. ^{31}P NMR (400 MHz, CD_2Cl_2): 298 K: δ = 64.27 (s, PPh_3); 223 K: δ = 50.45 (s, PPh_3), 53.90 (s, PPh_3), 66.76 (s, PPh_3), 68.82 (s, PPh_3), 73.79 (s, PPh_3), 79.73 (s, PPh_3), 82.50 (s, PPh_3), 83.58 (s, PPh_3) ppm. IR [ν(CO)/cm^{-1}; CH_2Cl_2]: $\tilde{\nu}$ = 1972 w, 1993 s, 2015 m, 2051 s. FAB-MS [M^+]: *m*/*z* = 2907. $C_{83}H_{62}Au_4O_{11}Os_4P_4$ (2908.12): calcd. C 34.28, H 2.15; found C 34.2, H 2.1.

Reaction of 1 with [$AuPPh_3Cl$] in Excess Et_3N: A solution of **1** (96 mg, 0.06 mmol) and excess [$AuPPh_3Cl$] in dichloromethane was stirred at room temperature. To this yellow solution, excess Et_3N was added dropwise to give a dark orange red solution. After stirring for 3 h, decomposition of products was observed. The solvent was then removed in vacuo. The residue was then subjected to TLC separation using *n*-hexane/dichloromethane (1:1, v/v) as the eluent. Three bands were obtained in the order of elution as **3** (17 mg, 14%), **4** (33 mg, 24%), and **6** (24 mg, 14%).

Reaction of 2 with [$AuPPh_3Cl$] in Excess Et_3N: To a yellow solution of **2** (32 mg, 0.02 mmol) and excess [$AuPPh_3Cl$] in dichloromethane, excess Et_3N was added. The yellow solution changed to orange after stirring for 3 h, accompanied by some decomposition prod-

ucts. The solvent was reduced under reduced pressure and the residue was chromatographed on silica with *n*-hexane/dichloromethane (1:1, v/v) as the eluent. Cluster **6** (7 mg, 12%) was isolated in moderate yield together with some unchanged **2** (12 mg, 0.008 mmol).

Reaction of 3 with [AuPPh$_3$Cl] in Excess Et$_3$N: An orange sample of **3** (40 mg, 0.02 mmol) and excess [AuPPh$_3$Cl] were mixed in dichloromethane. Excess Et$_3$N was added and the resultant orange solution was stirred at ambient temperature for 4 h. The solvent was reduced under reduced pressure and the residue was subjected to preparative TLC with *n*-hexane/dichloromethane (1:1, v/v) as the eluent. Two consecutive orange bands were identified as **4** (14 mg, 31%) and **6** (10 mg, 17%).

Reaction of 4 with [AuPPh$_3$Cl] in Excess Et$_3$N: An orange solution of **4** (47 mg, 0.02 mmol) and excess [AuPPh$_3$Cl] in dichloromethane were stirred with excess Et$_3$N for 6 h. No observable change could be detected, but a slight decomposition of starting material occurred.

Reaction of 5 with [AuPPh$_3$Cl] in Excess Et$_3$N: The reactivity of **5** cannot be thoroughly studied due to the limited availability of sample.

Reaction of 6 with [AuPPh$_3$Cl] in Excess Et$_3$N: A red solution of **6** (32 mg, 0.01 mmol) and excess [AuPPh$_3$Cl] were mixed in dichloromethane. Excess Et$_3$N was added and the resulting solution was stirred for an additional 6 h; purple insoluble microcrystalline precipitates appeared. These solids were confirmed as mixed-metal clusters with an Os/Au ratio of 3:2 by Energy Dispersive X-ray Analysis with SEM. IR [ν(CO)/cm^{-1}; KBr]: $\tilde{\nu}$ = 1952 m, 1979 s.

Catalytic Reactions: The catalytic reactions were performed inside a Parr high-pressure stainless steel reactor (100 mL) with internal magnetic stirring. The methanol, aniline, catalysts and promoters were charged into the reaction vessel. The reactor was sealed with six cap screws in a split-ring cover clamp. The air in the vessel was replaced with dinitrogen by 3 freeze-pump-thaw cycles. It was ensured that there was no leakage of gas. The reaction gas (CO and O_2) was then introduced into the reactor inside the fumehood. The reactor was heated to the preset temperature with a thermoregulated heater for a preset time period. At the end of the reaction, the reactor was cooled with an ice bath in order to quench the reaction immediately and the reaction gas was evacuated in the fumehood. The resulting liquid mixture was analyzed by GC and GC-MS with an HP 5890A and G1800C GCD Series II, respectively.

Electrochemical Studies: Electrochemical measurements were performed with an EG&G Princeton Applied Research (PAR) Model 273A potentiostat, connected to an interfaced computer employing PAR 270 electrochemical software. Cyclic volatmmograms and bulk electrolyses were carried out in a gas-tight cell consisting of three chambers that were separated at the bottom by fine frits equipped with a glassy carbon (Bioanalytical) or a carbon cloth (80 mm^2) working electrode, a platinum gauze auxiliary electrode (Aldrich), and an Ag/AgNO$_3$ reference electrode (Bioanalytical) at room temperature; 0.1 M *n*-tetrabutylammonium hexafluorophosphate (TBAHFP) in anhydrous deoxygenated acetonitrile was used as a supporting electrolyte. Ferrocene was added at the end of each experiment as an internal standard. The working potential (E_w) for redox processes was ca. 0.15 V more positive/negative than the corresponding electrode potential (E_p); the coulometric experiment was performed in duplicate.

X-ray Crystallographic Study: Single crystals were grown from their appropriate solvent systems under favorable conditions. Intensity data were collected at ambient temperature using a Bruker SMART 1K CCD diffractometer with graphite-monochromated Mo-K_α radiation using ω scans. Details of the intensity data collection and crystal data are given in Table 4, and selected bond lengths and angles are listed in Table 5. The data were corrected for Lorentz and polarization effects. The structures were solved by direct methods (SIR92[39] or SHELXS-86[40]), and expanded using Fourier techniques (DIRDIF94).[41] Some non-hydrogen atoms were refined anisotropically, while the rest were refined isotropically. Hydrogen atoms were included but not refined. All calculations were

Table 4. Crystal data and data collection parameters for **2** and **4**−**6**

	2	**4**	**5**	**6**
Empirical formula	$C_{32}H_{27}NO_{11}PAuOs_4$	$[C_{65}H_{47}O_{11}P_3Au_2Os_4]\cdot CHCl_3$	$C_{65}H_{48}O_{11}P_3Au_3Os_4$	$[C_{83}H_{62}O_{11}P_4Au_4Os_4]\cdot 2CHCl_3$
Formula mass	1590.31	2371.11	2449.71	3146.71
Crystal color, habit	Red, block	Red, plate	Red, block	Red, plate
Crystal dimensions [mm]	0.24 × 0.21 × 0.10	0.33 × 0.22 × 0.05	0.19 × 0.17 × 0.11	0.35 × 0.39 × 0.05
Crystal system	orthorhombic	triclinic	monoclinic	monoclinic
Space group	*Pbca* (no. 61)	$P\bar{1}$ (no. 2)	$P2_1/n$ (no. 14)	$P2_1/c$ (no. 14)
a [Å]	10.359(1)	12.157(1)	20.094(3)	14.789(2)
b [Å]	18.232(2)	14.377(1)	14.974(2)	24.768(3)
c [Å]	41.268(3)	23.463(2)	23.129(4)	24.760(3)
α [Å]	90	94.63(2)	90	90
β [Å]	90	93.04(2)	103.16(1)	96.10(1)
γ [Å]	90	90.14(2)	90	90
V [Å^3]	7793(1)	4081.7(6)	6776(1)	9018(1)
Z	8	2	4	4
D_c [g cm^{-3}]	2.710	1.929	2.401	2.317
μ(Mo-K_α) [cm^{-1}]	168.46	99.95	140.82	124.16
Reflections collected	49414	25597	42348	56388
Unique reflections	9763	17728	15893	18512
Observed reflections [$I > 1.5\sigma(I)$]	1471	9071	2149	2564
R	0.0323	0.0615	0.0443	0.0432
R_w	0.0305	0.0754	0.0529	0.0449
Goodness of fit *S*	1.143	1.735	1.556	1.437

Table 5. Selected bond lengths [Å] and angles [°] for **2** and **4**−**6**

	2	**4**	**5**	**6**
Os(1)−Os(2)	2.944(2)	2.897(1)	2.978(3)	3.002(2)
Os(1)−Os(3)	3.009(2)	2.832(1)	2.814(3)	2.992(2)
Os(1)−Os(4)	2.803(2)	2.973(1)	2.974(2)	2.798(2)
Os(2)−Os(3)	3.012(2)	2.796(1)	2.888(3)	2.929(2)
Os(2)−Os(4)	2.816(2)	3.006(1)	2.802(3)	2.806(3)
Os(3)−Os(4)	2.965(2)	3.017(1)	2.778(3)	2.775(2)
Au(1)−Os(1)	2.768(2)	2.742(1)	2.749(2)	2.783(2)
Au(1)−Os(2)	2.753(2)			
Au(1)−Os(2)		2.883(1)		
Au(2)−Os(1)		2.751(1)	2.744(3)	2.745(2)
Au(2)−Os(2)		2.789(1)		
Au(3)−Os(1)			2.759(2)	2.726(2)
Au(4)−Os(1)				2.820(2)
Au(1)−Au(2)		3.055(1)	2.796(3)	2.898(2)
Au(2)−Au(3)			2.860(2)	2.874(2)
Au(1)−Au(3)			2.804(2)	2.810(2)
Au(2)−Au(4)				2.804(2)
Au(3)−Au(4)				3.069(2)
Au(1)−P(1)	2.281(8)		2.25(1)	2.265(10)
Au(1)−P(2)		2.300(6)		
Au(2)−P(2)			2.26(1)	2.283(10)
Au(2)−P(3)		2.309(6)		
Au(3)−P(3)			2.26(1)	2.24(1)
Au(4)−P(4)				2.33(1)
Os(4)−P(1)		2.362(6)		
Os(3)−N(1)	2.24(2)			
Os(1)−Au(1)−Os(2)	64.47(4)			
Os(1)−Au(1)−Os(4)		63.76(3)		
Os(1)−Au(2)−Os(2)		63.05(3)		
Os(1)−Au(4)−Os(2)				62.80(5)
Au(2)−Au(1)−Os(1)		56.36(3)		
Au(2)−Au(1)−Os(4)		82.54(3)		
Au(1)−Os(1)−Au(2)		67.57(3)	61.20(6)	
Au(1)−Os(1)−Au(3)			61.21(6)	
Au(2)−Os(1)−Au(3)			62.62(6)	

performed using the teXsan[42] crystallographic software package of Molecular Structure Corporation. CCDC-194826 to -194829 contain the supplementary crystallographic data for this paper. These data can be obtained free of charge at www.ccdc.cam.ac.uk/conts/retrieving.html [or from the Cambridge Crystallographic Data Centre, 12 Union Road, Cambridge CB2 1EZ, UK; Fax: (internat.) + 44-1223/336-033; E-mail: deposit@ccdc.cam.ac.uk].

Acknowledgments

We gratefully acknowledge financial support from the Hong Kong Research Grants Council and the University of Hong Kong. Y. L. acknowledges the receipt of a postgraduate studentship (1999−2002) and the Li Po Chun Scholarship (2001−2002) administered by the University of Hong Kong and the Sir Edward Youde Memorial Fellowship (2001−2002) awarded by the Sir Edward Youde Memorial Trustees.

[1] J. Lewis, P. R. Raithby, in: *Metal Clusters In Chemistry* (Eds.: P. Braunstein, L. A. Oro, P. R. Raithby), Wiley-VCH, Weinheim, **1999**, pp. 348−380.
[2] I. Salter, in: *Comprehensive Organometallic Chemistry II* (Eds.: E. W. Abel, F. G. A. Stone, G. Wilkinson), Pergamon Press, Oxford, **1995**, vol. 10, pp. 255−322.
[3] A. J. Amoroso, J. Lewis, P. R. Raithby, W. T. Wong, in: *The Chemistry of the Copper and Zinc Triads* (Eds.: A. J. Welch, S. K. Chapman), The Royal Society of Chemistry, Cambridge, **1993**, pp. 202−206.
[4] Z. Ahkter, A. J. Edwards, S. L. Ingham, J. Lewis, A. M. Martin Castro, P. R. Raithby, G. P. Shields, *J. Clust. Sci.* **2000**, *11*, 217−226.
[5] Z. Ahkter, J. F. Gallagher, J. Lewis, P. R. Raithby, G. P. Shields, *J. Organomet. Chem.* **2000**, *614*−*615*, 231−237.
[6] A. J. Amoroso, M. A. Beswick, C. K. Li, J. Lewis, P. R. Raithby, M. C. Ramirez de Arellano, *J. Organomet. Chem.* **1999**, *573*, 247−253.
[7] Z. Ahkter, S. L. Ingham, J. Lewis, P. R. Raithby, *J. Organomet. Chem.* **1998**, *550*, 131−139.
[8] C. M. Hay, N. E. Leadbeater, J. Lewis, P. R. Raithby, K. Burgess, *New J. Chem.* **1998**, *22*, 787−788.
[9] Z. Akhter, S. L. Ingham, J. Lewis, P. R. Raithby, *Angew. Chem. Int. Ed. Engl.* **1996**, *35*, 992−993.
[10] C. Cathey, J. Lewis, P. R. Raithby, M. C. Ramirez de Arellano, *J. Chem. Soc., Dalton Trans.* **1994**, 3331−3332.
[11] Z. Akhter, S. L. Ingham, J. Lewis, P. R. Raithby, *J. Organomet. Chem.* **1994**, *474*, 165−171.
[12] M. M. Harding, B. Kariuki, A. J. Mathews, A. K. Smith, P. Braunstein, *J. Chem. Soc., Dalton Trans.* **1994**, 33−36.
[13] B. F. G. Johnson, F. J. Lahoz, J. Lewis, N. D. Prior, P. R. Raithby, W.-T. Wong, *J. Chem. Soc., Dalton Trans.* **1992**, 1701−1708.
[14] C. M. Hay, B. F. G. Johnson, J. Lewis, N. D. Prior, P. R. Raithby, W. T. Wong, *J. Organomet. Chem.* **1991**, *401*, C20−C22.
[15] R. Hoffmann, *Angew. Chem. Int. Ed. Engl.* **1982**, *21*, 711−724.
[16] L. Pignolet, in: *Catalysis by Di- and Polynuclear Metal Cluster Complexes* (Eds.: R. D. Adams, F. A. Cotton), Wiley-VCH, New York, **1998**, pp. 95−126.
[17] P. Braunstein, J. Rose, in: *Metal Clusters in Chemistry* (Eds.: P. Braunstein, L. A. Oro, P. R. Raithby), Wiley-VCH, Weinheim, Germany, **1999**, vol. 2, pp. 616−677.
[18] R. Pierantozzi, K. J. McQuade, B. C. Gates, M. Wolf, H. Knozinger, W. Ruhmann, *J. Am. Chem. Soc.* **1979**, *101*, 5436−5438.
[19] J. Evans, J. X. Gao, *J. Chem. Soc., Chem. Commun.* **1985**, 39−40.
[20] M. A. Aubart, B. D. Chandler, R. A. T. Gould, D. A. Krogstad, M. F. J. Schoondergang, L. H. Pignolet, *Inorg. Chem.* **1994**, *33*, 3724−3734.
[21] M. A. Aubart, L. H. Pignolet, *J. Am. Chem. Soc.* **1992**, *114*, 7901−7903.
[22] L. H. Pignolet, M. A. Aubart, K. L. Criaghead, R. A. T. Gould, D. A. Krogstad, J. S. Wiley, *Coord. Chem. Rev.* **1995**, *143*, 219−263.
[23] L. I. Rubinstein, L. H. Pignolet, *Inorg. Chem.* **1996**, *35*, 6755−6762.
[24] M. A. Aubart, J. F. D. Koch, L. H. Pignolet, *Inorg. Chem.* **1994**, *33*, 3852−3854.
[25] Y. Li, W. X. Pan, W. T. Wong, *J. Cluster Sci.* **2002**, *13*, 223−233.
[26] B. F. G. Johnson, D. A. Kaner, J. Lewis, P. R. Raithby, M. J. Taylor, *Polyhedron* **1982**, *1*, 105−107.
[27] M. R. A. Al-Mandhary, J. Lewis, P. R. Raithby, *J. Organomet. Chem.* **1997**, *536*, 549−551.
[28] Y. Li, W. T. Wong, *J. Cluster Sci.* **2001**, *12*, 595−617.
[29] C. M. Hay, B. F. G. Johnson, J. Lewis, R. C. S. Mcqueen, P. R. Raithby, R. M. Sorrell, M. J. Taylor, *Organometallics* **1985**, *4*, 202−205.
[30] K. P. Hall, B. R. C. Theobald, D. I. Guilmour, D. M. P. Mingos, A. J. Welsh, *J. Chem. Soc., Chem. Commum.* **1982**, 528−530.
[31] L. J. Farrugia, M. J. Freeman, M. Green, A. G. Orpen, F. G. A. Stone, I. D. Salter, *J. Organomet. Chem.* **1983**, *249*, 273−288.

[32] S. R. Bunkall, H. D. Holden, B. F. G. Johnson, J. Lewis, G. N. Pain, P. R. Raithby, M. J. Taylor, *J. Chem. Soc., Chem. Commum.* **1984**, 25−27.
[33] K. Burgess, B. F. G. Johnson, J. Lewis, P. R. Raithby, *J. Chem. Soc., Dalton Trans.* **1983**, 1661−1665.
[34] J. A. K. Howard, I. D. Slater, F. G. A. Stone, *Polyhedron* **1984**, *3*, 567−573.
[35] D. D. Perrin, W. L. F. Armarego, *Purification of Laboratory Chemicals*, 4th ed., Butterworth-Heinemann, Oxford, **1996**.
[36] H. D. Kaesz, S. A. R. Knox, J. W. Koepke, R. B. Saillant, *J. Chem. Soc., Chem. Commun.* **1971**, 477.
[37] B. F. G. Johnson, J. Lewis, P. R. Raithby, G. M. Scheldrick, K. Wong, *J. Chem. Soc., Dalton Trans.* **1978**, 673−676.
[38] C. Zuccaro, G. Pampaloni, F. Calderazzo, *Inorg. Synth.* **1989**, *26*, 293−295.
[39] SIR92: A. Altomare, G. Cascarano, C. Giacovazzo, A. Guagliardi, *J. Appl. Crystallogr.* **1993**, *26*, 343−350.
[40] SHELXS 86, Program for Crystal Structure Solution: G. M. Sheldrick, *Acta Crystallgr., Sect. A* **1990**, *46*, 467−473.
[41] DIRDIF94: P. T. Beurskens, G. Admiraal, G. Beurskens, W. P. Bosman, R. de Gelder, R. Israel, J. M. M. Smits, *The DIRDIF-94 program system*, Technical Report of the Crystallography Laboratory, University of Nijmegen, The Netherlands, **1994**.
[42] TeXsan: Crystal Structure Analysis Package, Molecular Structure Corporation, The Woodlands, TX, USA, **1985** and **1992**.

Received December 27, 2002

